Supporting Information

Improved Cyclic Performance of Si Anodes for Lithium-Ion Batteries by Forming Intermetallic Interphases between Si Nanoparticles and Metal Microparticles

Xingkang Huang,[†] Haihui Pu,[†] Jingbo Chang,[†] Shumao Cui,[†] Peter B. Hallac,[‡] Junwei Jiang,[‡] Patrick T. Hurley,[‡] and Junhong Chen[†]*

† Department of Mechanical Engineering, University of Wisconsin-Milwaukee, 3200 N Cramer Street, Milwaukee, WI 53211, USA.

‡ Global Technology & Innovation, Power Solutions, Johnson Controls, 5757 N Green Bay Avenue, Milwaukee, WI 53209, USA

Experimental Section

Nickel powders (spherical, ≈ 5-15 micron, 99.0%), copper powders (spherical, ≈ 10 micron, 99.9%), and iron powders (spherical, 1-3 micron, 98+%) were purchased from Alfa Aesar and used directly without further purification.

Si/M (M= Ni, Cu, Fe, etc.) composites were synthesized typically by mixing nano-sized Si powders (crystalline, 98%, Laser synthesized from vapor phase, Alfa Aesar) and micro-sized M powders in an agate mortar for 10 min and annealing the mixtures in a tube furnace (Lindberg/Blue M) under H_2/Ar with a flow rate of 200 mL min^{-1}. The furnace was quickly heated up to a given temperature (typically in 15-25 min), held at the temperature for 2 min for Si/Ni mixtures or 1 min for Si/Cu and Si/Fe mixtures, and cooled down quickly with the help of forced airflow by a fan. The weight ratio of Si/M was 1:3 to obtain a discharge capacity of around 700 mAh g^{-1} because an anode with a higher capacity than this value could not significantly improve the capacity of a full cell given a limited capacity of existing cathode materials.[1]

The as-prepared samples were characterized by powder X-ray diffraction (XRD) on a Scintag XDS 2000 diffractometer with Cu Kα radiation. Scanning electron microscopy (SEM) was performed on a Hitachi S-4800. X-ray photoelectron spectroscopy (XPS) spectra of samples were obtained using an HP5950A ESCA spectrometer with monochromatic Al Kα radiation as X-ray source. Charge/discharge performance was characterized by 2032-tpye coin cells that were assembled in an argon-filled glove box with contents of oxygen and moisture below 1 ppm. Electrodes were prepared by mixing the as-prepared Si/M composites as the active material, poly(acrylic acid) and carboxymethyl cellulose (1:1, w/w) as binders, and carbon black as a conductor with a weight ratio of 70:10:20 to form a slurry. The resulting slurries were coated onto a Cu foil using the doctor blade method. After drying and pressing, the Cu foil was cut into

disks (1.11 cm in diameter) with typical electrode material loadings of ca. 2 mg. 1 M $LiPF_6$ dissolved in ethylene carbonate/ethyl methyl carbonate (40:60, v/v) was employed as an electrolyte, with 10 wt.% fluoroethylene carbonate as an additive. Cyclic voltammetry (CV) and electrochemical impedance spectroscopy (EIS) of the as-prepared anodes were measured on a PARSTAT 4000 electrochemical station by using a three-electrode cell, with the Si/Ni composite electrode as a working electrode, a lithium disk as a counter electrode, and a lithium ring as a reference electrode. CV was carried out at a scanning rate of 0.1 mV s^{-1} while EIS was tested between 10,000-0.1 Hz with an amplitude of 10 mV.

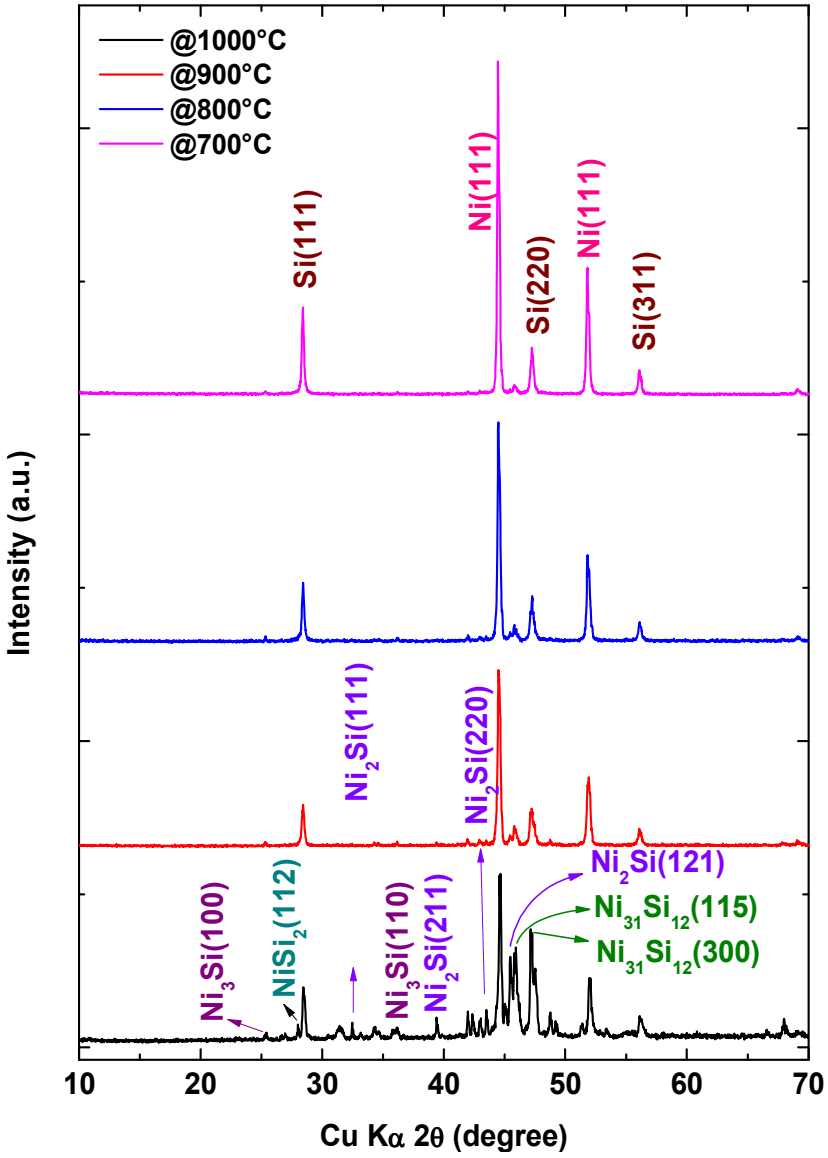

Figure S1 XRD patterns of Si/Ni composites obtained at various temperatures.

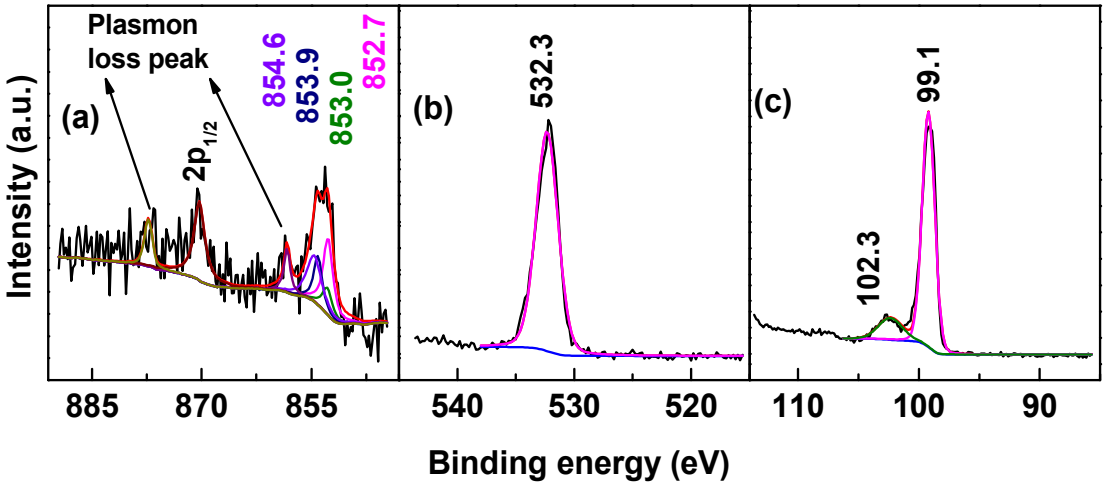

Figure S2. XPS spectra of Si/Ni composite obtained at 900 °C: (a) Ni 2p, (b) O 1s, and (c) Si 2p.

The Ni 2p peaks are complicated; the broad peak over a binding energy range of 850-857 eV is ascribed to nickel metal and silicides (Ni (852.7 eV), Ni_3Si (852.8 eV), $Ni_{31}Si_{12}$ (853.0 eV), Ni_2Si (853.4 eV), NiSi (853.9 eV), and $NiSi_2$ (854.6 eV)). The contents of Ni on the surface of the Si/Ni composite in forms of elemental Ni and silicides are 39.3% and 60.7%, respectively. We assigned the XPS peak at 857.3 eV to plasmon loss energy of Ni instead of Ni $2p_{3/2}$ because there is only one symmetrical peak at 532.3 eV for O 1s. This O 1s peak is ascribed to oxygen in the form of SiO_x because silicon oxide was detected as indicated by the Si 2p peak (102.3 eV). In contrast, the O 1s peak of NiO is located at 320 eV. We have added corresponding discussions on Page 6 of the revised manuscript.

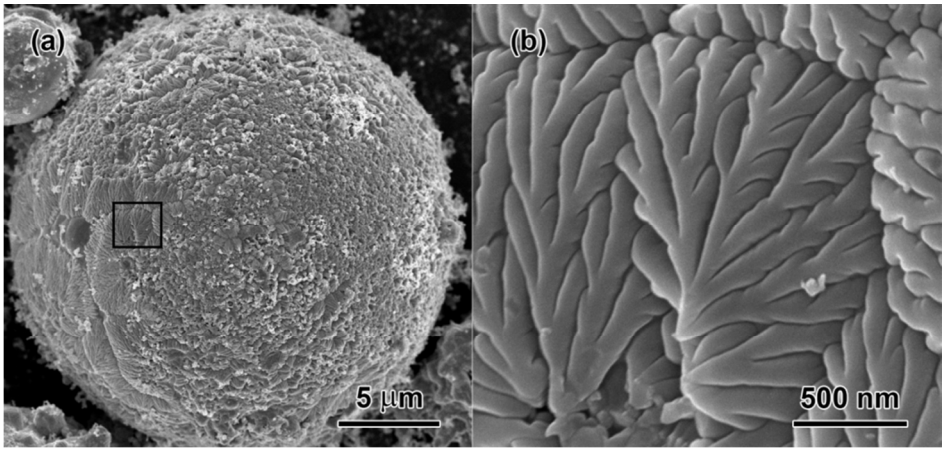

Figure S3 SEM image of the Si/Ni composite obtained at 1,000 °C.

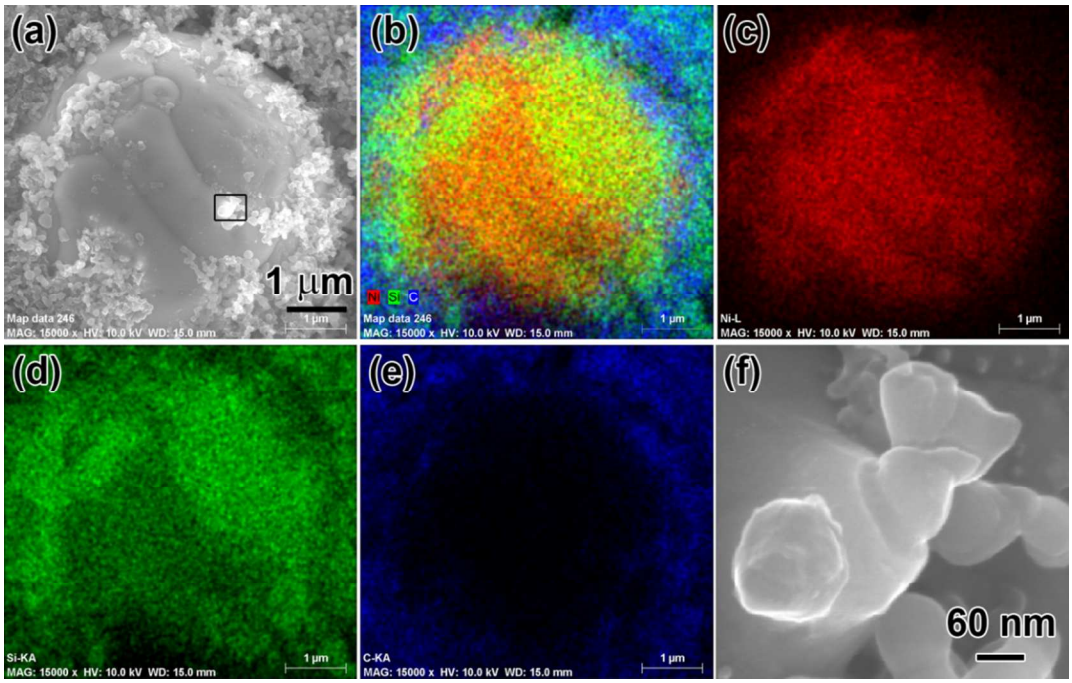

Figure S4 SEM images and EDS elemental mapping of the Si/Ni composite (from 900 °C) electrode after 10 cycles: (a) SEM image, and elemental mappings of (b) overlapping Ni, Si, and C, (c) Ni, (d) Si, and (e) C; (f) shows an enlarged SEM image corresponding with the marked area by a square in (a). From (a) and (b) we can see carbon surrounding the Ni particle, suggesting Ni particle does not lose physical contact with carbon while (f) indicates that Si is still attached onto the surface of the Ni particle after 10 cycles of charge and discharge.

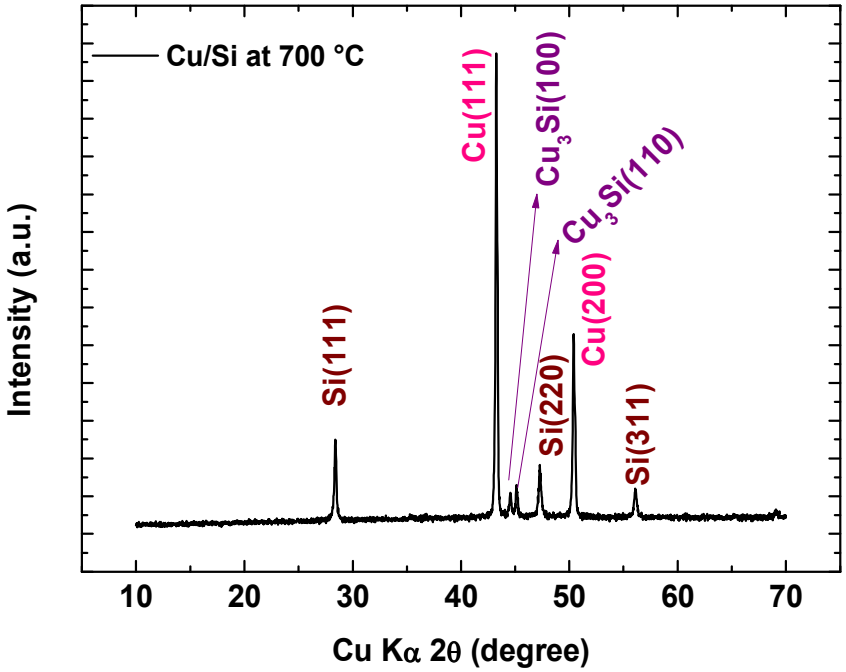

Figure S5 XRD pattern of the Cu/Si composite obtained at 700 °C.

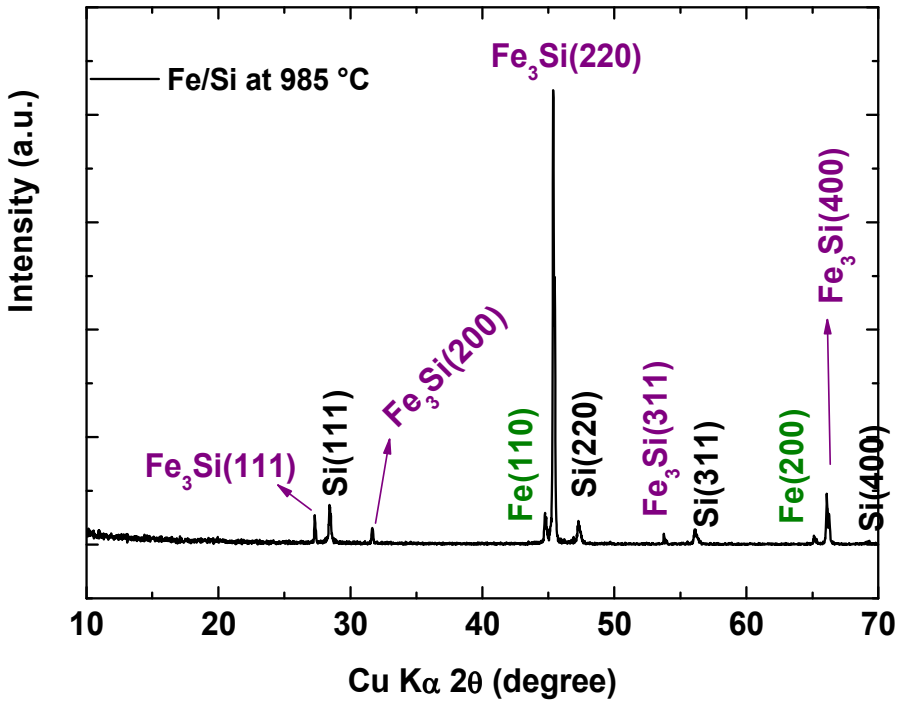

Figure S6 XRD pattern of the Si/Fe composite obtained at 980 °C by using a 1-3 μm spherical Fe powders.

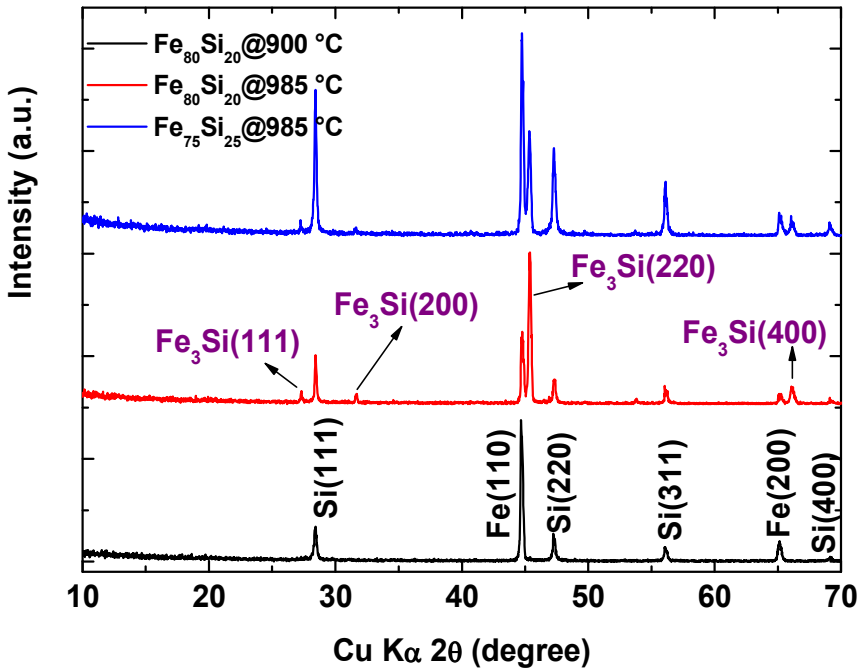

Figure S7 XRD pattern of Si/Fe composites. The sample with Si/Fe=1:4 (by weight) annealed at 900 °C does not show any peak of silicides. In contrast, the composites (Si/Fe=1:4 or 1:3, by weight) prepared at 985 °C exhibit peaks of Fe_3Si. Note here these results were obtained by using a regular Fe powder (+325 mesh) instead of spherical particles used in Figure S6.

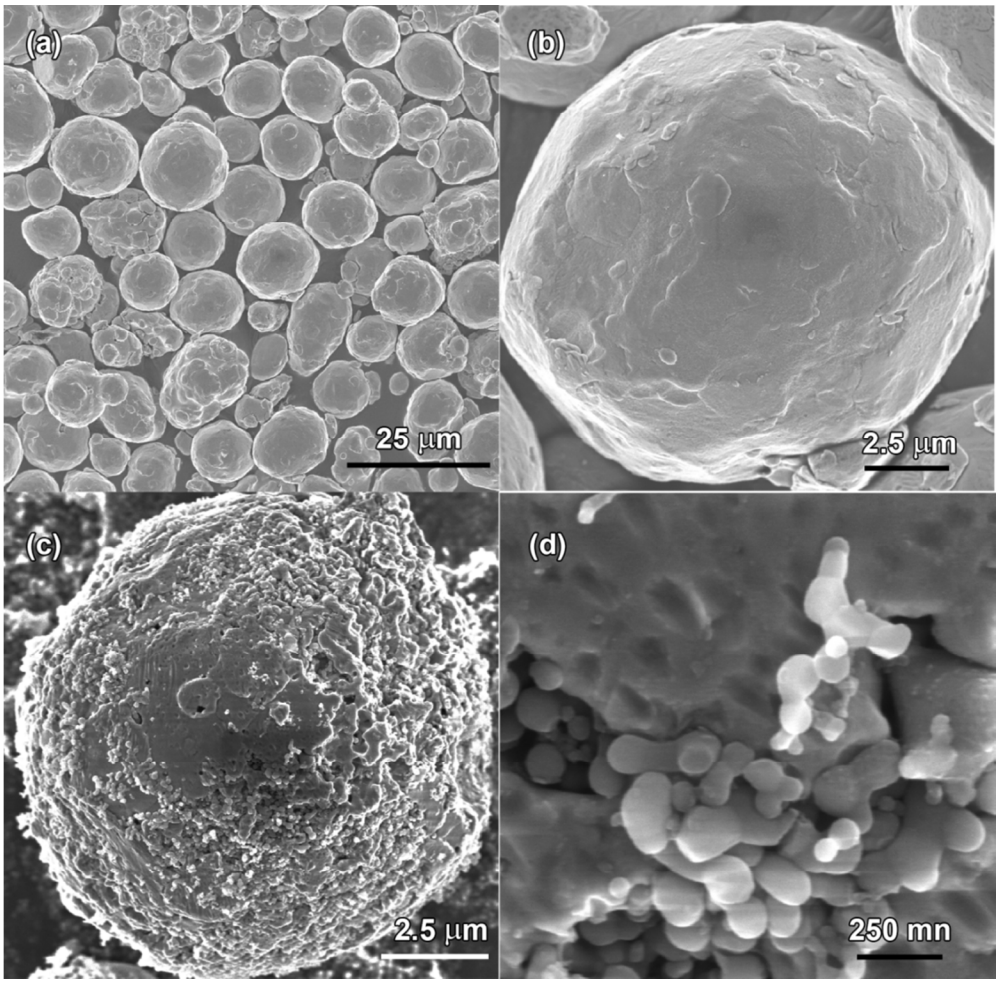

Figure S8 SEM images of (a-b) spherical Cu powders and (c-d) Si/Cu composites obtained at 700 °C with Si/Cu=1:3 (by weight).

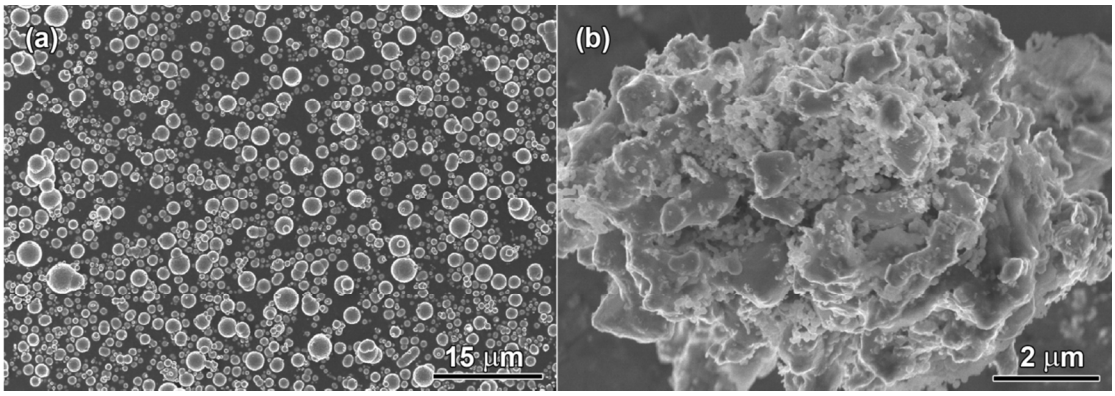

Figure S9 SEM images of (a) spherical Fe powders (1-3 μm) and (b) Si/Fe composites obtained at 985 °C with Si/Cu=1:3 (by weight).

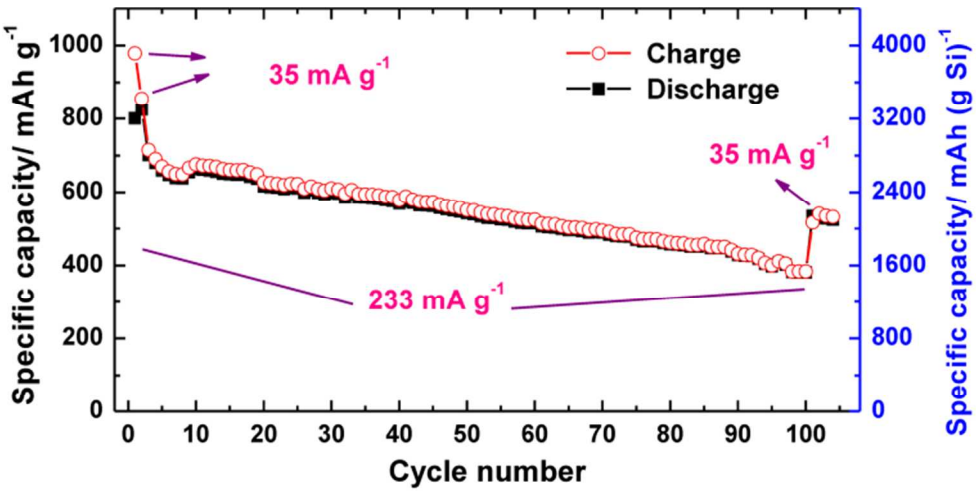

Figure S10. Cyclic performance of Si/Cu composite prepared at 700 °C.

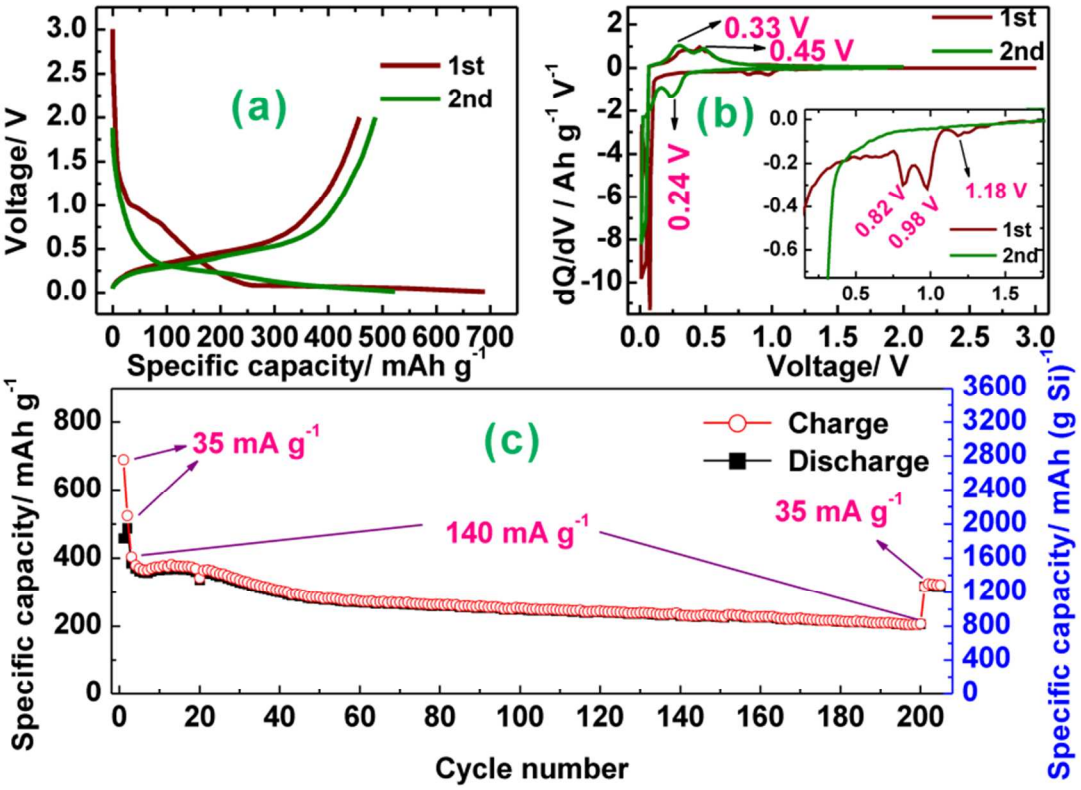

Figure S11. (a) Initial charge/discharge curves of the Si/Fe composite prepared at 985 °C, (b) its differential capacity plots, and (c) its cyclic performance.

For the Si/Fe composite, its capacity was ca. 487 mAh g^{-1} (Figure S11), much lower than those of Si/Ni and Si/Cu composites. This is because the Si/Fe composite was synthesized at 985 °C, below which iron silicide was not observed (Figure S7); at that high temperature, Si reacted with Fe very quickly, resulting in a high content of intermetallic phases and a low content of elemental Si. The initial Coulombic efficiency of the Si/Fe composite is 66.4%, much lower than that of the Si/Ni and Si/Cu composites. A potential plateau at about 0.9 V is observed on the initial charge curve of the Si/Fe composite anode (Figure S11a), and disappears in the subsequent cycles. The differential capacity plot (Figure S11b) shows three peaks at 1.17, 0.98, and 0.88 V; the first one results from the SEI formation while the latter two peaks may be due to the reduction of iron

oxides formed when the Si/Fe composite was exposed in air during the electrode fabrication. Although such an Si/Fe composite delivered a much lower capacity than Si/Ni and Si/Cu composites, it possesses a better cyclic performance. As shown in Figure S11c, it delivered 386 mAh g^{-1} at 140 mA g^{-1}, which decayed to 281 mAh g^{-1} at the 50^{th} cycle and remained at 205 mAh g^{-1} (820 mAh (g Si)$^{-1}$ afterwards. The decaying rates before and after the 50^{th} cycle are 2.2% and 0.51% each cycle, respectively. The relatively faster degradation rate during the initial stage might be associated with the fact that not all the Si is welded to Fe particles. The free Si loses electrical contact with binders and conductors more easily compared with those welded onto Fe particles. After this stage, those well-attached Si performed much more stably. When the current density recovered to 35 mA g^{-1}, the Si/Fe composite still could deliver 319 mAh g^{-1} (i.e., 1,276 mAh (g Si)$^{-1}$), 65.6% of its highest capacity at the second cycle.

Reference:

(1) Kasavajjula, U.; Wang, C. S.; Appleby, A. J. *J. Power Sources* **2007,** *163*, 1003-1039.

(2) Cao, Y.; Nyborg, L.; Jelvestam, U. *Surf. Interface Anal.* **2009,** *41*, 471-483.